Phonon scattering and energy relaxation in two-, one-, and zero-dimensional electron gases

U. Bockelmann
Laboratoire de Physique de la Matière Condensée de l'Ecole Normale Supérieure, 24 rue Lhomond, F-75005 Paris, France and Walter Schottky Institut, Technische Universität München, D-8046 Garching bei München, Germany

G. Bastard
Laboratoire de Physique de la Matière Condensée de l'Ecole Normale Supérieure, 24 rue Lhomond, F-75005 Paris, France
(Received 25 May 1990)

We report on calculations of intrasubband and intersubband phonon scattering in quantum-confined electron gases based on lattice-matched $In_xGa_{1-x}As/InP$ quantum wells. Dimensionality effects on the emission of acoustic phonons are studied comparing the scattering times of two-, one-, and zero-dimensional electron gases as a function of the lateral confinement. Optical phonon scattering in quantum wells and wires is discussed using a phenomenological broadening of the one-dimensional density of states. The energy relaxation rates of heated electron gases due to phonon emission and absorption have been calculated for lattice temperatures T_l between 0.3 and 20 K. For a given heating power per electron, the electron temperature T_e in a quantum wire can be greater or smaller than that in the corresponding quantum well, depending on the electron density n_s, while the energy relaxation in quantum dots with significant quantization energies is always slower than in the corresponding wells and wires.

The investigation of two-dimensional electron gases (2DEG) in semiconductors (quantum wells, heterostructures, metal oxide semiconductors, etc.) and the improvement of growth techniques have given rise to a lot of new physical effects as well as device applications. Progress in nanofabrication makes it possible to reduce further the dimensionality by laterally structuring the 2DEG and realizing a quantum confinement in two (quantum wire) or even all three (quantum dot) directions of space. With these exists at least the potential for new interesting quantum effects comparable to the transition from three to two dimensions.

The electronic states in all solid structures are subject to different scattering mechanisms. While the influence of imperfections (impurities, layer-width fluctuations) can, at least in principle, be controlled by improved technology, phonon scattering is inherent to the solid state of matter. Concerning the hot carriers, the emission of phonons is often the only important nonradiative relaxation mechanism because impurity scattering is mostly elastic. The scattering of a 2DEG by longitudinal-acoustic (LA) and -optical (LO) phonons has already been studied theoretically by several groups (see, e.g., Refs. 1–5). The investigation of one-dimensional structures has focused on the LO phonons[4–8] that are important for device applications at room temperatures, while LA phonon scattering[8,9] has received less attention. To our knowledge the phonon scattering in quantum dots has not yet been calculated. We have calculated the interaction of LA and LO phonons with electron gases of reduced dimensionality and compare the two-, one-, and zero-dimensional (2D, 1D, and 0D, respectively) structures systematically.

In order to be quantitative in view of possible future experiments we have used the parameters of the following semiconductor system. A rectangular $In_{0.47}Ga_{0.53}As$ quantum well with a width of 100 Å embedded in InP serves as the two-dimensional basis. The lateral confinement is modeled by potential barriers of infinite height outside the wire or dot region. This particular choice of the confinement potential results in a complete separation of the carrier motion in the three spatial directions. The wave functions in the growth direction (z) are the solutions of the finite-barrier Ben Daniel–Duke quantum-well problem,[10] which are harmonic functions $[\sin(k_w z),\cos(k_w z)]$ inside the well matched to exponential decreasing tails $[\exp(-k_b z)]$ in the barriers. In the lateral directions we have used either harmonic wave functions restricted to the confined region or plane waves to describe the propagation along the unconfined direction(s). It is assumed that the spectrum of longitudinal phonons consists of one isotropical acoustic (LA) and two dispersionless optical (LO) branches since $In_{1-x}Ga_xAs$ is a two LO mode alloy. In using the bulk phonons of $In_{0.47}Ga_{0.53}As$ we neglect any change of the phonon spectrum due to the presence of the InP barriers or lateral structure. This approach is based on the large ratio of electron and phonon quantum-confinement energies[11] which scale like $m_{\rm ion}/m_e$.

Electron-phonon scattering times τ are calculated in first-order perturbation theory using the Fermi golden rule,

$$\tau_{i\to f}^{-1}=\frac{2\pi}{\hbar}\sum_{f,\mathbf{q}}\alpha^2(q)|\langle\psi_f|e^{\mp i\mathbf{q}\cdot\mathbf{r}}|\psi_i\rangle|^2 \times\delta(E_f-E_i\pm E_q)[n_B(E_q,T_l)+\{{}^{1}_{0}\}] . \quad (1)$$

The upper (lower) signs account for emission (absorption) of phonons by an electron in the initial quantum state i. The sum extends over all possible final-electron quantum

numbers f (i and f comprise subband and wave-vector coordinates) and phonon wave vectors $\mathbf{q}$. The electron energies E_i and E_f are always measured from the bottom of the respective 0D, 1D, or 2D ground subbands. N_B stands for the Bose distribution function $n_B(E,T)=(e^{(E/kT)}-1)^{-1}$. E_q is the energy of a phonon with wave vector $\mathbf{q}$ and T_l is the lattice temperature.

For the coupling of the electron to LA phonons by means of a deformation potential D, the expression

$$\alpha^2(q)=\frac{D^2}{2\rho c_s^2\Omega}\hbar c_s q \tag{2}$$

is used with $D=7.2$ eV, a density $\rho=5500$ kg/m^3, and a longitudinal velocity of sound $c_s=3400$ m/s. Piezoelectric coupling to acoustic phonons is expected to be weaker than the deformation-potential coupling by about a factor of 10 (Refs. 3 and 12) in the range of our calculations. The strength of the (Fröhlich) interaction between the electron and the two LO branches is described[13] by

$$\alpha_i^2(q)=\frac{c_i}{\Omega q^2}\ ,$$
$$c_1=\frac{2\pi e^2\hbar\omega_{L1}}{\epsilon_\infty}\left[1-\frac{\omega_{T1}^2}{\omega_{L1}^2}\right]\frac{\omega_{T2}^2-\omega_{L1}^2}{\omega_{L2}^2-\omega_{L1}^2}\ , \tag{3}$$
$$c_2=\frac{2\pi e^2\hbar\omega_{L2}}{\epsilon_\infty}\left[1-\frac{\omega_{T2}^2}{\omega_{L2}^2}\right]\frac{\omega_{L2}^2-\omega_{T1}^2}{\omega_{L2}^2-\omega_{L1}^2}\ .$$

For the energies of the two longitudinal- ($\hbar\omega_{L1},\hbar\omega_{L2}$) and transverse- ($\hbar\omega_{T1},\hbar\omega_{T2}$) optical branches we use 28.9, 33.6, 28.2, and 31.9 meV, respectively. The electron-phonon matrix element in Eq. (1) separates in the x,y,z coordinates and has been calculated analytically. For a confined lateral direction (for instance, x) the following expression holds:

$$|\langle\varphi_x^n|e^{iq_x x}|\varphi_x^{n'}\rangle|^2=M_x^{n,n'}(q_x)$$
$$=\frac{1}{4}\left[\frac{\sin(Q+K_i+K_f)}{Q+K_i+K_f}+\frac{\sin(Q+K_i-K_f)}{Q+K_i-K_f}\pm\frac{\sin(Q-K_i+K_f)}{Q-K_i+K_f}\pm\frac{\sin(Q-K_i-K_f)}{Q-K_i-K_f}\right]^2\ , \tag{4}$$

with $Q=q_xL_x/2$, $K_i=n\pi/2$, $K_f=n'\pi/2$. The upper signs stand for the band index n and n' both even or odd, the lower signs are for one of them even and the other odd. Concerning the z direction we have obtained an expression similar to Eq. (4) with a small additional contribution caused by the leakage of the wave function into the finite barriers. As seen from Eq. (4) $M_x^{n,n'}(q_x)$ decreases rapidly with increasing $q_xL_x\gg1$ [the increasing number of oscillations of $\exp(iq_xx)$ inside the well of width L_x results in a decreasing interaction]. For small q_x it approaches zero and unity for interband ($n\neq n'$) and intraband ($n=n'$) transitions, respectively. In free directions the matrix element reduces to the conservation of the crystal momentum [$\delta(k_i-k_f+q)$].

After taking advantage of the δ functions, which stand for the conservation of the crystal momentum in the nonconfined directions and the total energy, we have evaluated Eq. (1) numerically for LA phonon scattering. Figure 1 shows the rates τ^{-1} for LA phonon emission by an electron at a lattice temperature T_l of 4 K. We have chosen the same energy difference E_i between the initial and the lowest electron state for the quantum dot (0D), the quantum wire (1D), and the quantum well (2D), as illustrated in the inset. The initial electron states are the first excited level and the edge of the first excited subband of the dot and the wire, respectively. The corresponding 2D situation is an electron of energy

$$E_i=\hbar^2/2m^*(\pi/L)^2(2^2-1^2)$$

in the ground quantum-well subband. Consequently, we deal with intersubband scattering in 0D and 1D and intrasubband scattering in the 2D structure. When the lateral size L exceeds 2000 Å the three scattering rates decrease monotonously and become very close. This demonstrates the disappearance of any physical difference between the zero-, one-, and two-dimensional systems when the lateral confinement becomes weak. In this range the deformation-potential interaction weakens due to the decreasing phonon wave vector $\mathbf{q}$ [Eq. (2)]. In

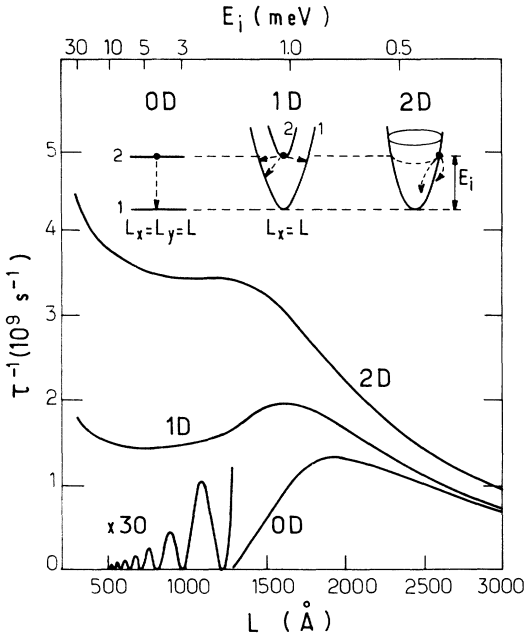

FIG. 1. Emission rates of LA phonons from zero- (0D), one- (1D), and two- (2D) dimensional electron gases. L (lower scale) indicates the lateral layer width(s) and defines the initial energy E_i (upper scale). The 0D scattering rates plotted below 1300 Å are multiplied by a factor of 30. $T_l=4$ K.

addition for 1D and 2D the number of available final electron states decreases.

Phonon scattering in a quantum well conserves the total energy and the in-plane crystal momentum. For a given phonon energy an increase of the in-plane momentum transfer results in a decrease of the phonon impulsion in the confined direction and hence an increase of the scattering probability. Final states with $\mathbf{k}_f \cong -\mathbf{k}_i$ exhibit the greatest contribution. Thus, increasing E_i increases k_i and consequently the phonon scattering rate τ^{-1}. The decrease of τ_{1D}^{-1} (1D) with L below 600 Å has a similar shape and can be explained along the same line as before. The maximum at $L=1600$ Å indicates the enhanced density of states for energies at the 1D subband edges. The maximum appears at that initial energy E_i for that it is most probable that the electron ends up at the ground subband edge. In the 1D and 2D cases there always exists a continuum of final electron states and possible phonon energies. The quantum dot system has only the ground state available below E_i. Thus, the emitted LA phonon spectrum consists of a single line with $q=E_i/\hbar c_s$. For L below ~ 1300 Å (E_i above ~ 2 meV) τ_{0D}^{-1} is smaller than τ_{1D}^{-1} and τ_{2D}^{-1} by more than one order of magnitude and exhibits strong oscillations. The relevant quantity of the electron-phonon interaction in a confined direction i is $q_i L_i$ [Eq. (4)]. For a given $q \gg L_i^{-1}$ a quantum dot emits LA phonons preferentially in the direction with the strongest confinement (here z). The same holds for a quantum wire concerning the LA phonon interaction in the two confined (x,z) directions. Consequently, the oscillations in τ_{0D}^{-1} are governed by the factor $\sin^2(q_z L_z)$ from Eq. (4) and have a constant period in $L^{-2} \sim E_i \sim q \cong q_z$.

Figure 2 shows the rate τ^{-1} and the mean phonon energy $\langle E_{ph} \rangle$ for the emission of LA phonons by a quantum wire as a function of its lateral width L. Here the initial electron is located 5 meV above the edge in the ground subband. The corresponding 2D values do not depend on L and are indicated by long bars. Multiplying by $E_q=\hbar c_s q$ before the summations are performed in Eq. (1) gives the energy-loss rate P of the electron gas. The plotted mean phonon energy results from $\langle E_{ph} \rangle = P\tau$. For L below 750 Å only intrasubband scattering in the ground subband is possible. With increasing L the energy separations between different subbands decrease and more and more subband edges move below E_i, opening additional intersubband scattering channels. Any appearance of a new subband is clearly observable because its density of states is enhanced in comparison with the other subbands due to the peaked density of states at the band edge $[g_{1D}(E) \sim (E-E_{edge})^{-1/2}]$. There τ^{-1} increases rapidly but continuously, reaching a maximum

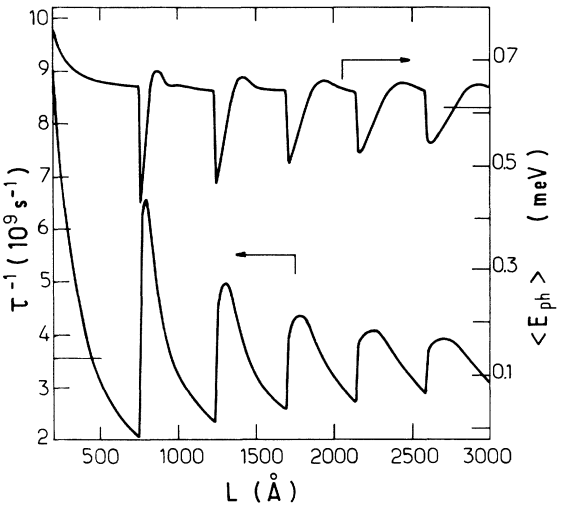

FIG. 2. Emission rate τ^{-1} (lower curve, left scale) and mean energy $\langle E_{ph} \rangle$ (upper curve, right scale) of LA phonons emitted by an electron in the ground 1D subband with an initial energy of 5 meV as a function of the lateral wire width L. The long bars mark the corresponding 2D results. $T_l=4$ K.

when E_i is about 0.6 meV above the edge of the new subband. $\langle E_{ph} \rangle$ exhibits a sharp minimum followed by a weak maximum because the energy difference $E_i - E_{edge}$ increases from zero to values that are larger than the mean phonon energy for scattering into the other available final subbands. The influence of a new subband weakens with a growing number of occupied subbands. As before the 1D curves approach the 2D values with increasing L.

In contrast to the acoustic phonons discussed up to now, the optical phonons have no continuous-energy spectrum in our dispersionless approach. For the 0D system the discrete electrons and LO phonon energies prevent any first-order (Fröhlich) interaction, except for the special cases $E_i - E_j = \hbar\omega_{LO}$. A finite scattering time can result from broadening of the electron and phonon spectra, renormalization of the phonons due to the confinement, and higher-order interaction terms (for instance, the simultaneous interaction with a LA and a LO phonon). The following calculations are restricted to one- and two-dimensional systems. The assumption that E_{ph} does not depend on q allows us to analytically calculate Eq. (1) for LO phonons to a greater extent. For emission of phonons of the jth ($j=1,2$) branch, we obtain ($kT_e \ll \hbar\omega_{LJ}$)

$$\tau_{1D}^{-1}(E_i)=c_j \frac{m^*}{4\pi^2\hbar^3}\frac{1}{k_f}\int_0^\infty dq\, q \left[\frac{1}{q^2+(k_i-k_f)^2}+\frac{1}{q^2+(k_i+k_f)^2}\right]\int_0^{2\pi} d\varphi\, M_x^{n,n'}(q\cos\varphi) M_z^{l,l'}(q\sin\varphi)\ , \tag{5a}$$

$$\tau_{2D}^{-1}(E_i)=c_j \frac{m^*}{\pi\hbar^3}\int_0^\infty dq \frac{M_z^{l,l'}(q)}{[(k_f^2+k_i^2+q^2)^2-4k_f^2k_i^2]^{1/2}}\ , \tag{5b}$$

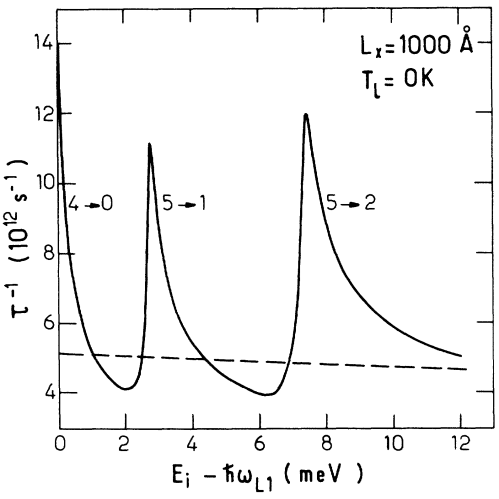

FIG. 3. Scattering rates τ^{-1} of 1D (solid) and 2D (dashed) electron gases due to the emission of phonons of the lowest LO branch ($\hbar\omega_{L1}$=28.9 meV). Above the 1D curve the relevant 1D subband transitions are indicated. The lateral wire width L_x is 1000 Å and T_l=0 K.

where k_i (k_f) is the modulus of the wave vector for an electron with the energy E_i (E_f) in the respective 1D or 2D initial (final) subband. Here τ_{1D}^{-1} exhibits singularities when k_f equals zero in contrast to the smooth curves obtained for the deformation potential coupling to LA phonons. The ratio of the unbroadened density of states of one subband in 1D and 2D is

$$g_{1D}/g_{2D}=2/(L_x k) . \tag{6}$$

From this point of view it becomes clear that $\tau_{1D}^{-1}(E_i)$ has a similar shape as $g_{1D}(E_i-\hbar\omega_{LO})$, exhibiting singularities at the 1D subband edges. In real 1D systems g_{1D} is smooth due to broadening effects. The formula

$$g_{1D}(E)=g_{2D}\left[1+2\sum_{n=1}^{\infty}J_0(2\pi n\gamma)e^{-n/n_0}\right] \tag{7}$$

describes phenomenologically the broadened density of states of all subbands[14] where

$$\gamma=\{1+E[\hbar^2\pi^2/(2m^*L_x^2)]^{-1}\}^{1/2}$$

and J_0 is a Bessel function of the first kind (here n_0=5 results in a broadening Γ of about 1 meV). Instead of adding the individual scattering rates for all possible transitions between broadened initial and final 1D subbands, we calculate τ_{1D}^{-1} approximately as follows. By means of Eq. (6) we introduce the broadened density of states [Eq. (7)] into Eq. (5a) and calculate the matrix element between the initial and final subbands, which exhibit the greatest density of states at a given E_i. Each time the relevant initial or final 1D subband changes we match the scattering rates continuously over the range of the broadening using a cubic polynom. Figure 3 shows the resulting rates for emission of LO phonons as a function of E_i for the 1D (solid) and the 2D (dashed) systems.

To know about the energy relaxation of heated carriers at low temperatures is important, in particular for the interpretation of optical experiments. The energy-loss rates P of the 2DEG in GaAs/$Al_{1-x}Ga_xAs$ heterostructures have been extracted from Shubnikov–de Haas measurements[12,15] at electron temperatures below 20 K and agree well with calculations[3] for LA phonons interacting by means of a deformation potential. To calculate the energy loss in the $In_{1-x}Ga_xAs$/InP system we add the rates of emission (P_{LAe}) and absorption (P_{LAa}) of LA phonons and the emission of the two different types of LO phonons (P_{LO1},P_{LO2}),

$$P(\mu,T_e,T_L)=\int_0^{\infty}dE_i g(E_i)n_F(E_i,T_e,\mu)[P_{LAe}(E_i,T_L,T_e,\mu)-P_{LAa}(E_i,T_L,T_e,\mu)+P_{LO1}(E_i,T_e,\mu)+P_{LO2}(E_i,T_e,\mu)] . \tag{8}$$

Here n_F is the Fermi-Dirac distribution function of the electron gas

$$n_F(E,T,\mu)=(e^{[(E-\mu)/kT]}+1)^{-1} .$$

For the energy-loss rates of the two types of LO phonons there is

$$P_{LOj}(E_i,T_e,\mu)=\tau_{LOj}^{-1}(E_i)\hbar\omega_{Lj}[1-n_F(E_i-\hbar\omega_{Lj},T_e,\mu)] \tag{9}$$

with $\tau_{LO}^{-1}(E_i)$ as in Fig. 3. The term $[1-n_F(\cdots)]$ describes the occupation and therefore suppression of final states by the other electrons. P_{LAe} and P_{LAa} result from Eq. (1) when the term under the sum is multiplied by $\hbar c_s q[1-n_F(E_i-\hbar c_s q,T_e,\mu)]$. If an electron gas is heated (for example, by an applied electric field) its temperature T_e increases above the lattice temperature T_l until the heating power equals the overall energy-loss rate $P(\mu,T_e,T_l)$. The use of the Fermi-Dirac distribution function excludes strong electric fields and supposes that the electron-electron scattering rate exceeds the electron-phonon scattering rate in order to establish the thermal equilibrium of the heated electron gas.

Figure 4 presents T_e for 1D (solid) and 2D (dashed) electron gases with the same areal density n_s as a function of the heating power per electron P for several values of T_l. The 1D and 2D curves are similar, showing the expected increase of T_e with P. The LO phonon emission is negligible below 20 K, but dominates the relaxation above about 30 K. The onset of significant electron heating shifts to higher P with increasing T_l because the relaxation strengthens with the growing number of LA phonons. Nevertheless, T_e increases with T_l for any heating power P.

Figure 5 shows the density dependence of the energy-

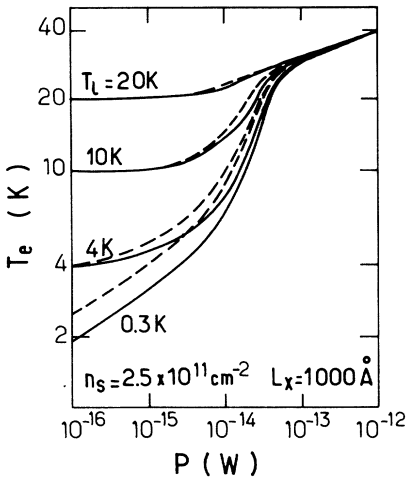

FIG. 4. Electron temperature T_e of 1D (solid) and 2D (dashed) electron gases as a function of the heating power per electron P for different lattice temperatures T_l. The lateral wire width L_x is 1000 Å and the areal electron density n_s is 2.5×10^{11} cm^{-2} (the corresponding 1D density is 2.5×10^{6} cm^{-1}).

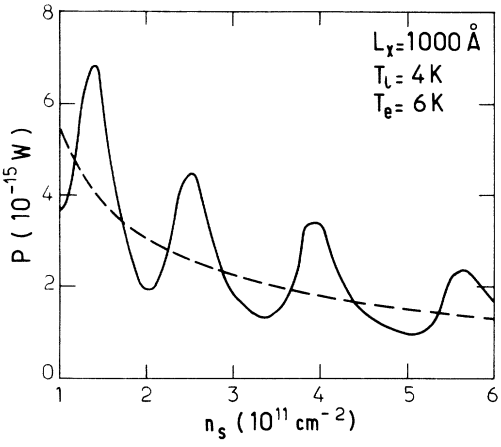

FIG. 5. Energy-loss rates P per electron of 1D (solid) and 2D (dashed) electron gases as a function of the areal electron density n_s at a lattice temperature T_l of 4 K and an electron temperature T_e of 6 K. The lateral wire width L_x is 1000 Å.

loss rates for fixed electron and lattice temperatures. The energy-loss rate per electron P decreases with increasing n_s because the number of states in the energy shell of width kT_e around μ that are available for scattering in a degenerate electron gas does not grow proportionally to n_s. The 1D energy-loss rate oscillates around the 2D curve exhibiting maxima when μ lies slightly above a 1D subband edge. Consequently, the relaxation in 1D can be faster or slower than in the corresponding 2D structure. Figure 4 is an example for the first situation.

Finally, the energy relaxation of a single electron in a quantum dot can be compared to that in quantum wires and wells using Figs. 1 and 2. For L below $\sim$1300 Å ($E_i \gtrsim 2$ meV) the energy-loss rate of an electron in 0D $\tau_{0D}^{-1}E_i$ is smaller than 10^8 meV/s (Fig. 1), while the order of magnitude of the corresponding quantity $\tau^{-1}\langle E_{ph}\rangle$ is 10^9 meV/s for 1D and 2D systems (Fig. 2). Thus, for quantization energies above $\sim$2 meV the energy relaxation by LA phonons is generally slower in the 0D than in the 1D and 2D structures.

In conclusion, we have discussed LA and LO phonon scattering and the associated relaxation properties of two-, one-, and zero-dimensional electron gases. A simple approximation to the LO phonon-scattering rates of a multisubband 1D system, including broadening effects, has been presented. In the 1D systems the calculated quantities of the phonon scattering (scattering rates τ^{-1}, mean LA phonon energies $\langle E_{ph}\rangle$, energy-loss rates P) exhibit oscillations around their corresponding 2D values, which are characteristic of the 1D density of states. On the other hand, the LA phonon scattering in 0D systems becomes increasingly quenched with increasing quantization energies.

We would like to thank R. Ferreira for helpful discussions. One of us (U.B.) acknowledges financial support from the "Deutsche Forschungs Gemeinschaft (DFG)" via the Leibniz fund. This work has been partly supported by the "Ministère de la Recherche et de la Technologie."

[1]P. J. Price, Ann. Phys. (N.Y.) **133**, 217 (1981).
[2]R. Ferreira and G. Bastard, Phys. Rev. B **40**, 1074 (1989).
[3]Y. Okuyama and N. Tokuda, Phys. Rev. B **40**, 9744 (1989).
[4]F. A. Riddoch and B. K. Ridley, Surf. Sci. **142**, 260 (1984).
[5]J. P. Leburton, J. Appl. Phys. **56**, 2850 (1984).
[6]A. Ghosal, D. Chattopadhyay, and A. Bhattacharyya, J. Appl. Phys. **59**, 2511 (1986).
[7]B. G. Mulimani, C. H. Ramakrishna, B. S. Krishnamurthy, and C. K. Sarkar, Phys. Status Solidi B **156**, 253 (1989).
[8]S. Briggs and J. P. Leburton, Phys. Rev. B **38**, 8163 (1988).
[9]V. K. Arora, Phys. Rev. B **23**, 5611 (1981).
[10]G. Bastard, *Wave Mechanics Applied to Semiconductor Heterostructures* (Les Editions de Physique, Les Ulis, 1988).
[11]S. Schmitt-Rink, D. A. B. Miller, and D. S. Chemla, Phys. Rev. B **35**, 8113 (1987).
[12]K. Hirakawa and H. Sakaki, Appl. Phys. Lett. **49**, 889 (1986).
[13]L. Swierkowski, W. Zawadzki, Y. Guldner, and C. Rigaux, Solid State Commun. **27**, 1245 (1978).
[14]G. Bastard, J. A. Brum, and R. Ferreira (unpublished).
[15]S. J. Manion, M. Artaki, M. A. Emanuel, J. J. Coleman, and K. Hess, Phys. Rev. B **35**, 9203 (1987).